The Company of **Biologists**

RESEARCH ARTICLE

Krox20 defines a subpopulation of cardiac neural crest cells contributing to arterial valves and bicuspid aortic valve

Gaëlle Odelin[1], Emilie Faure[1], Fanny Coulpier[2,3], Maria Di Bonito[4], Fanny Bajolle[5], Michèle Studer[4], Jean-François Avierinos[1,6], Patrick Charnay[2,3], Piotr Topilko[2,3] and Stéphane Zaffran[1,*]

ABSTRACT

Although cardiac neural crest cells are required at early stages of arterial valve development, their contribution during valvular leaflet maturation remains poorly understood. Here, we show in mouse that neural crest cells from pre-otic and post-otic regions make distinct contributions to the arterial valve leaflets. Genetic fate-mapping analysis of Krox20-expressing neural crest cells shows a large contribution to the borders and the interleaflet triangles of the arterial valves. Loss of *Krox20* function results in hyperplastic aortic valve and partially penetrant bicuspid aortic valve formation. Similar defects are observed in neural crest *Krox20*-deficient embryos. Genetic lineage tracing in *Krox20*$^{-/-}$ mutant mice shows that endothelial-derived cells are normal, whereas neural crest-derived cells are abnormally increased in number and misplaced in the valve leaflets. In contrast, genetic ablation of *Krox20*-expressing cells is not sufficient to cause an aortic valve defect, suggesting that adjacent cells can compensate this depletion. Our findings demonstrate a crucial role for *Krox20* in arterial valve development and reveal that an excess of neural crest cells may be associated with bicuspid aortic valve.

KEY WORDS: Neural crest, Cardiac development, *Krox20*, Mouse, Genetics, Bicuspid aortic valve, *Egr2*

INTRODUCTION

Heart valve development occurs through an epithelial-to-mesenchymal transition (EMT) process (Eisenberg and Markwald, 1995; Person et al., 2005). The development of arterial (or semilunar) valves is differentiated from that of atrioventricular valves by the contribution of migrating neural crest cells (de Lange et al., 2004; Lincoln et al., 2004). Multipotent neural crest cells (NCCs) originate from the margins of the neural plate and migrate throughout the body (reviewed by Sauka-Spengler and Bronner, 2010). In the head, they give rise to the mesectoderm, a particularly multipotent mesenchyme with the ability to give rise to skeletal and perivascular structures in addition to ectodermal derivatives (Le Lievre and Le Douarin, 1975). The caudal (post-otic) population of mesectoderm is known as the vagal or cardiac neural crest, although it also gives rise to most enteric ganglia (Kuratani and Kirby, 1991;

Le Douarin and Teillet, 1973). Cardiac NCCs delaminate from the dorsal hindbrain, from the middle of the otic vesicle to the caudal border of the first somites, corresponding to rhombomeres (r) 6, 7 and 8. These cells migrate ventrally through pharyngeal arches 3, 4 and 6 to reach the arterial pole of the heart. NCCs are necessary for aortic arch artery remodeling and outflow tract (OFT) septation (Kirby et al., 1983). Recent studies have demonstrated that neural crest is particularly important for arterial valve formation (Jain et al., 2011; Nakamura et al., 2006; Phillips et al., 2013). Although the contribution of cardiac NCCs to the arterial valve is evident, their role in human disease pathogenesis remains unclear.

Bicuspid aortic valve (BAV) is the most common congenital heart defect with a prevalence estimated at 1% (Hinton and Yutzey, 2011; Hoffman and Kaplan, 2002). The BAV is often isolated but may be also associated with other congenital malformations, including coarctation of the aorta, interruption of the aortic arch, patent ductus arteriosus or isolated ventricular septal defect, suggesting a common etiology between these cardiac defects (Siu and Silversides, 2010). Although usually asymptomatic at birth, BAV predisposes to valvular dysfunctions, such as aortic stenosis and/or insufficiency, which may require treatment and/or surgery (Fedak et al., 2002; Garg, 2006). Despite the frequency and potential morbidity of BAV, our understanding of the mechanism underlying this congenital malformation remains limited.

We recently reported that the zinc-finger transcription factor Krox20 (Egr2 – Mouse Genome Informatics) is a crucial activator of fibrillar *Col1a1* and *Col3a1* genes during valve development (Odelin et al., 2014). Here, we provide evidence that post-otic NCCs expressing *Krox20* migrate through the 3rd pharyngeal arch to later invest murine arterial valves. Previous studies have shown that *Krox20* is transcribed in r3 and r5, but not in other part of the neural tube, and that its deletion results in alteration of the antero-posterior positional identity of r3 and r5 (Schneider-Maunoury et al., 1993; Wilkinson et al., 1989). Using various transgenic mouse lines, we compared neural crest origins and showed segregated distribution of their derivatives in the arterial valve leaflets. Loss of *Krox20* function results in abnormal development of the aortic valve, which in 30% generates a BAV phenotype. Similar defects are observed in neural crest *Krox20*-deficient embryos. Genetic fate-mapping analysis in *Krox20*$^{-/-}$ showed that additional neural crest-derived cells are found in the leaflets of the aortic valve. In addition, we used different transgenic mice to examine the contribution of pre-otic and post-otic NCCs in aortic valve development. Our study identifies an essential role for *Krox20*-expressing NCCs during arterial valve formation and disease.

RESULTS

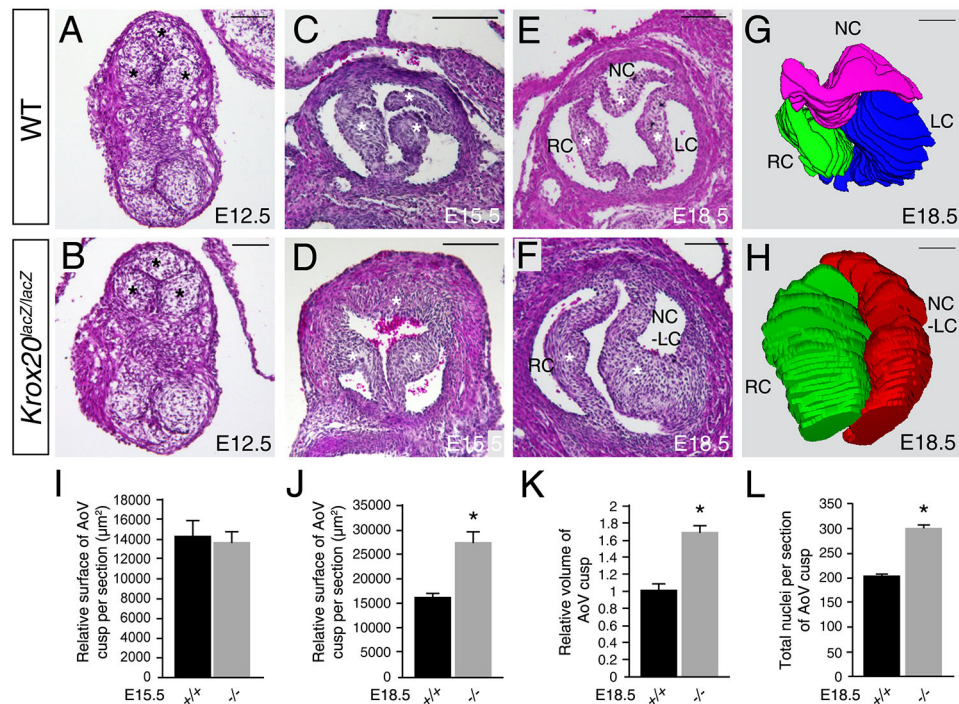### Homozygous disruption of *Krox20* results in bicuspid aortic valves

We have already shown that *Krox20* mutant mice have aortic valve dysfunction associated with disorganization of the extracellular

DEVELOPMENT

Fig. 1. *Krox20* **mutant mice display bicuspid aortic valves.** (A-F) Cross-sectional Hematoxylin and Eosin-stained images through the aortic valve leaflets of wild-type (A,C,E) and *Krox20^(lacZ/lacZ)* (B,D,F) littermate. At E12.5 (*n*=18) and E15.5 (*n*=14), no obvious difference is seen between wild-type (A,C) and *Krox20^(lacZ/lacZ)* (B,D) arterial valves. (I) At E15.5, the relative surface of the aortic valve leaflet per section is similar in wild-type and mutant embryos. (E,F) At E18.5, three aortic valve leaflets (asterisks) are observed in the wild-type embryo (E), whereas abnormal aortic valve with thickened and unequal-sized leaflets are detected in the mutant (F). Asterisks indicate valvular leaflets of the aortic valve. (G,H) Three-dimensional (3D) reconstructions of histological sections at E18.5. Wild-type embryo (G) has an aortic valve with three leaflets, each with three commissures, whereas a *Krox20^(-/-)* embryo (H) demonstrates an abnormal aortic valve with two leaflets. (J) The relative surface area of the aortic valve leaflet per section is significantly increased in the mutant compared with controls. (K) Quantification of the average volume of the aortic valve leaflet displays that mutant valves are 1.8 times larger than control valves. (L) The mean of total nuclei per leaflet shows a significant increase in the mutant aortic valve. All data were calculated from *n*=6 embryos for each genotype. Data are mean±s.e.m. (*$P<0.05$, Student's *t*-test). Left coronary (LC, blue), right coronary (RC, green), non-coronary (NC, purple) and fused left coronary-non coronary (LC-NC, red) leaflets. Scale bars: 100 µm.

matrix (Odelin et al., 2014). Here, we expand our analysis to the morphology of the valves from embryonic day (E) 12.5 to E18.5 (Fig. 1 and Fig. S1). No anomaly was detected at E12.5 (*n*=18) or E14-E15.5 (*n*=14) (Fig. 1A-D,I). At 18.5, all wild-type (*n*=32) embryos observed had normal tricuspid aortic valves comprising two coronary (RC and LC) and one non-coronary (NC) valve leaflets (Table 1; Fig. 1E). In contrast, all (22/22) *Krox20^(lacZ/lacZ)* (termed *Krox20^(-/-)*) fetuses had hypertrophic aortic valve leaflets and 27% of these (6/22) had developed bicuspid aortic valve (BAV) at E18.5 (Table 1; Fig. 1F). Of note, pulmonary valves and the great arteries were normal in both wild-type and *Krox20^(-/-)* embryos.

To characterize the type of BAV, we performed three-dimensional (3D) reconstructions of the aortic valve in wild-type and mutant fetuses. 3D reconstructions demonstrated that the phenotype of BAV in *Krox20^(-/-)* resulted from the fusion of the non-coronary leaflet with either the right or the left coronary leaflets (R-N or L-N) (Fig. 1G,H). We also observed a raphe between the non-coronary and the right coronary leaflets in 33% of the BAVs in *Krox20^(-/-)* (Table 1 and Fig. S1). Consistent with our previous observation (Odelin et al., 2014), quantification of the 3D volume or the measurement of the relative surface area showed that mutant valves were 1.8 times larger than the controls (Fig. 1J,K; *P*=0.0002, Student's *t*-test). The total number of mutant valvular cells was increased by 30% over that of the controls (Fig. 1L, *P*=0.014, Student's *t*-test). Interestingly, quantifications of these parameters in distinct leaflets revealed no significant differences between coronary and non-coronary leaflets in *Krox20^(-/-)* aortic valve (Fig. S1). Together, these results suggest that lack of *Krox20* perturbs the development of the aortic valve, and it is associated with bicuspid phenotype.

Table 1. Aortic valve anomalies in *Krox20^(-/-)* and conditional embryos at E18.5

Genotype	*n*	Hypertrophic AoV	Bicuspid AoV	Bicuspid with raphe
Wild type	32	0	0	0
Krox20^(-/-)	22	22	6 (27%)	2/6
Wnt1-Cre	29	0	0	0
Wnt1-Cre; Krox20^(flox/flox)	19	19	2 (10.5%)	2/2
Tie2-Cre; Krox20^(flox/flox)	20	0	2 (10.5%)	0/2
Krox20^(flox/+)	14	0	0	0
Krox20^(Cre/flox)	13	13	1 (8%)	0/1

n indicates number of scored embryos; AoV; aortic valve.

Fate-mapping of *Krox20*-derived cells in the arterial valves

At E9.5, *Krox20* expression is detected in r3 and r5, but also in NCCs originating from r5 (Fig. S2) (Ghislain et al., 2003; Schneider-Maunoury et al., 1993; Wilkinson et al., 1989). We used *Wnt1-Cre* and *Krox20^(Cre)* mice to perform a genetic lineage tracing of NCC populations during arterial valve formation. At E12.5 and E15.5, distinct valve leaflets were apparent, and

2

Wnt1-Cre-labeled cells were mostly present in the coronary leaflets of the aortic valve (Fig. 2A,B). At E18.5, all three aortic valve leaflets had contributions from NCC, even if fewer *Wnt1-Cre*-labeled cells were observed in the non-coronary compared with the coronary leaflets (Fig. 2C). Many NCC-derived cells were also detected at the insertion zone (attachment point) of the valve leaflets of *Wnt1-Cre;Rosa^{mTmG/+}* embryos (Fig. 2B,C, arrowheads). At this stage, the left and right leaflets of the pulmonary valve contained NCC-derived cells, whereas the anterior leaflet had very few NCC (Fig. 2D). To genetically fate-map the *Krox20*-expressing cells, we used a *Krox20^{Cre}* allele together with the *Rosa^{tdTomato}* reporter line (Madisen et al., 2010; Voiculescu et al., 2000). At E13.5, the three aortic leaflets contained *Krox20*-derived cells, although the non-coronary leaflet contained very few Tomato-positive cells (Fig. 2E). However, a substantial contribution to aortic valve structure was observed at E15.5 and E18.5 (Fig. 2F,G). Similar to *Wnt1-Cre*-labeled cells, *Krox20*-derived cells were located at the insertion zone of the valve leaflets (Fig. 2F,G; arrowheads). *Krox20*-expressing cells contribute also to the pulmonary valve leaflets, with a reduced

contribution to the anterior leaflet (Fig. 2H). Using the *Z/AP* reporter line, we examined the lineage of cells that expressed *Krox20* in E17.5 *Krox20^{Cre/+}* embryos. Valvulography confirmed a large contribution of *Krox20-Cre*-labeled cells at the borders and in the interleaflet triangles (RΔN, RΔL and LΔN) of the arterial valves (Fig. 2I-K). Endogenous expression of *Krox20* mRNA and proteins had been seen in a subset of mesenchymal cells of the aortic valve after E12.5 stage (Odelin et al., 2014). At E18.5, *Krox20* was expressed at the border of the aortic valve leaflets (Fig. S3). Immunostaining revealed several double Tomato/Krox20-positive cells in the aortic valve of *Krox20^{Cre};Rosa^{tdTomato}* embryos (Fig. S3). To examine the origin of these valvular cells, we performed further co-immunostaining in *Wnt1-Cre;Rosa^{mTmG/+}* and *Tie2-Cre;Rosa^{mTmG/+}* embryos. At E13.5 and later, Krox20 protein expression was detected in both NCC- and endothelial-derived cells (Fig. S3), suggesting different origins of Krox20-expressing cells during arterial valve development. These experiments demonstrate that *Krox20* is expressed in a subset of NCCs that make a substantial contribution to the arterial valves.
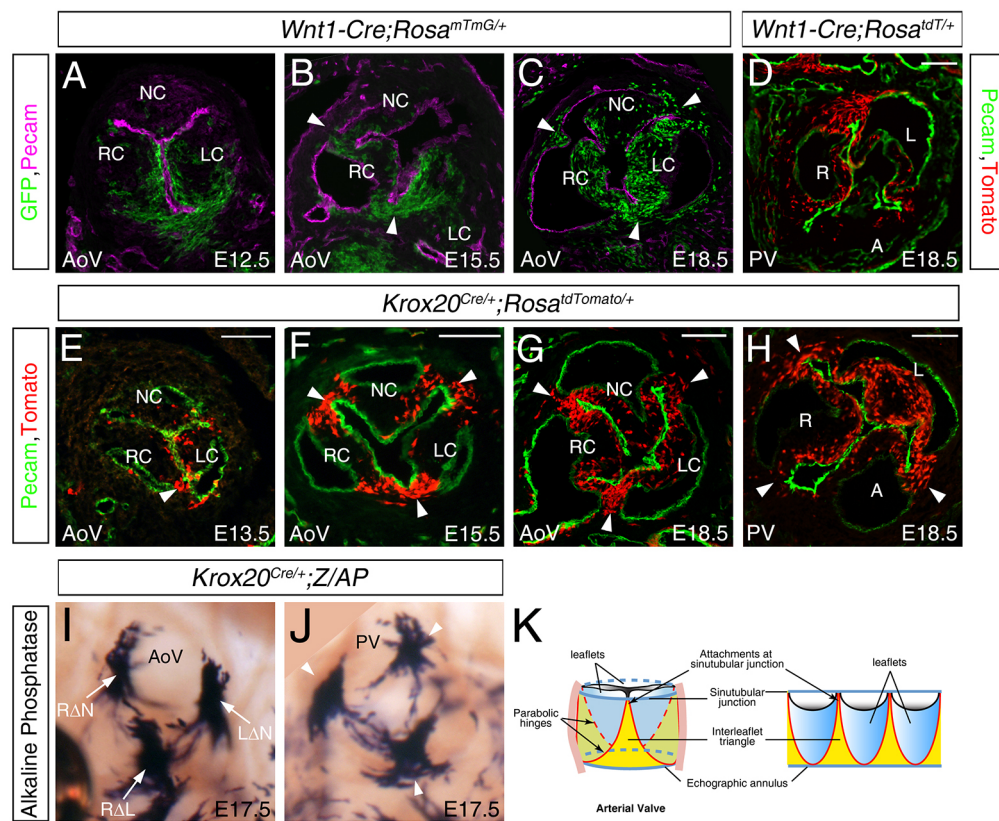
Fig. 2. Concordance of *Krox20-Cre* and neural crest labeling in the arterial valve. (A-D) Immunofluorescence staining of the arterial valves of *Wnt1-Cre; Rosa^{mTmG/+}* (A-C) and *Wnt1-Cre;Rosa^{tdTomato}* (D) embryos. The cell membrane-localized green fluorescence (GFP) reporter protein in Cre recombinase-expressing cells. GFP-reporter protein is in green and Pecam is labeled in purple. Immunofluorescence reveals expression of the reported protein (membrane-GFP; green) in the forming leaflets at E12.5 (A). (B,C) At E15.5 and E18.5, the GFP-positive cells are found in the three leaflets of the aortic valve. Contribution of NCCs is more abundant in both coronary leaflets than in the non-coronary leaflet. (D) The right (R) and left (L) leaflets of the pulmonary valve contain NCC-derived cells (Tomato; red), whereas the anterior (A) leaflet contains very few NCCs. (E-H) Immunofluorescence staining on the aortic valve of *Krox20^{Cre/+};Rosa^{tdTomato}* embryos. Tomato-reporter is in red and Pecam is labeled in green. Immunofluorescence reveals expression of the reported protein (Tomato; red) in a few cells at the base of the leaflets (arrowheads) at E13.5 (E). (F,G) By E13.5, *Krox20-Cre*-labeled cells are located the insertion zone of the valve leaflets and along each commissure. (H) The right and left leaflets of the pulmonary valve contain *Krox20*-derived cells; there are a few *Krox20-Cre*-labeled cells present in the anterior leaflet. (I,J) E17.5 hearts from *Krox20^{Cre/+};Z/AP* embryos were stained for alkaline phosphatase and treated to be transparent. Expression is detected in the insertion zone (attachments) of the aortic (AoV; I) and pulmonary (PV; J) valve leaflets, and in the interleaflet triangle regions (arrowheads). (K) Three- and two-dimensional representations of the arterial valve leaflets. The red lines correspond to the parabolic hinge of each leaflet. The interleaflet triangle is shown in yellow. LC, left coronary leaflet; NC, non-coronary leaflet; RC, right coronary leaflet; RΔN, right-non-coronary interleaflet triangle; RΔL, right-left interleaflet triangle. Scale bars: 100 μm.

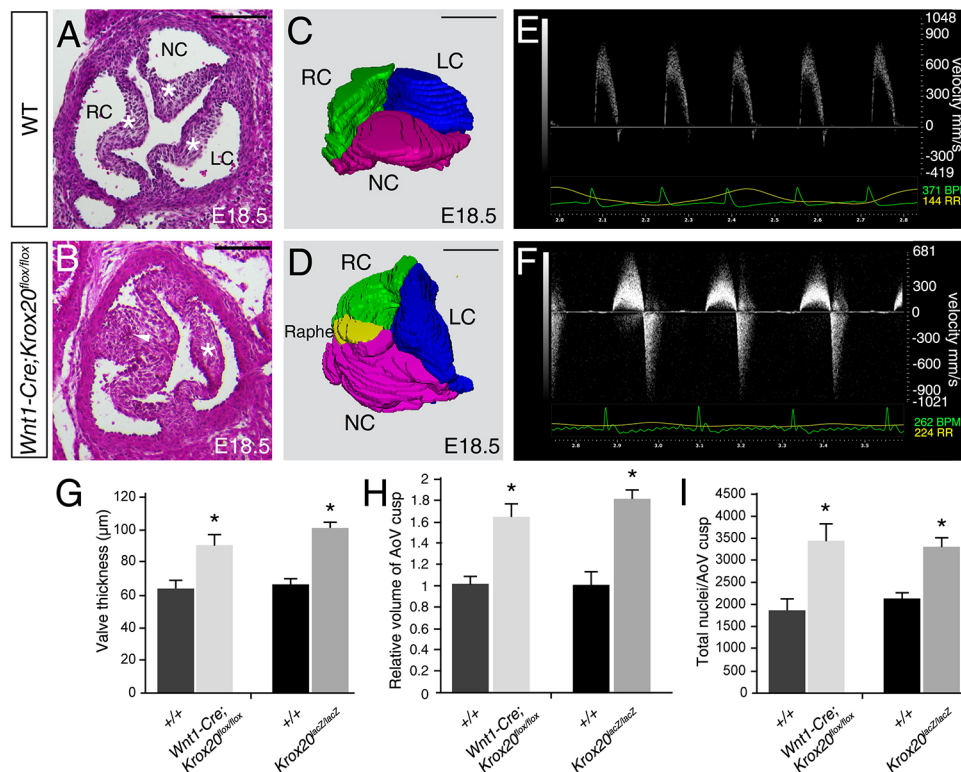## Deletion of *Krox20* in neural crest cells results in aortic valve defects

To investigate the role of *Krox20* in NCCs that contribute to arterial valve development, we used the *Krox20flox* allele together with the *Wnt1-Cre* line. *Wnt1-Cre;Krox20flox/flox* embryos were observed at the expected Mendelian ratio and newborn mice were viable. Because the *Wnt1-Cre* line was reported to cause developmental phenotype by ectopic activation of Wnt signaling (Lewis et al., 2013), we checked whether heterozygous *Wnt1-Cre* embryos had any valve defect. At E18.5, our observation revealed no valve defect in this genetic context (*n*=29; Table 1). However, examination of *Wnt1-Cre;Krox20flox/flox* fetuses at E18.5 revealed morphological anomalies of the aortic valve, including hyperplasic (19/19) and bicuspid (2/19) leaflets (Table 1; Fig. 3A,B). The phenotype of BAV observed in *Wnt1-Cre; Krox20flox/flox* resulted from the fusion between the non-coronary and the right coronary leaflets (Fig. 3A-D). To further assess cardiac function, we performed echocardiography on 1-month-old mice. Pulse-wave Doppler analysis of the aorta showed flow reversal in *Wnt1-Cre;Krox20flox/flox* (*n*=3) mice but not in wild type (*n*=3) (Fig. 3E,F). These results indicate that loss of *Krox20* function in the neural crest lineage leads to aortic valve dysmorphogenesis and aortic insufficiency.

Given that aortic valve leaflets in *Wnt1-Cre;Krox20flox/flox* embryos appeared enlarged (Fig. 3B,D), we performed a morphometric analysis at E18.5. The thickness of the aortic valve leaflets was confirmed by this analysis, which revealed an average 1.6 -old greater volume in *Wnt1-Cre;Krox20flox/flox* and *Krox20−/−* compared with wild-type littermates (Fig. 3G,H). Quantification of total number of aortic valve cells showed a significant increase of mesenchymal cell number in *Wnt1-Cre;Krox20flox/flox* and *Krox20−/−* compared with wild-type littermates (Fig. 3I), suggesting that increased cell number contributes to aortic valve leaflet enlargement in these mutant mice. Interestingly, we have previously shown that proliferation of valvular cells was not affected in *Krox20−/−* embryos at E13.5, E15.5 and E17.5 (Odelin et al., 2014), indicating that this defect is a proliferative-independent process. We next assessed whether there was a deficiency in apoptosis. At E13.5 and E17.5, counting of caspase 3-positive cells did not show any significant difference between wild-type (*n*=3 at each stage) and *Krox20−/−* (*n*=3) embryos (Fig. S4), indicating that cell death is not affected in the aortic valves of the mutant embryos.

Additional neural crest cell derivatives in *Krox20−/−* is associated with bicuspid aortic valve

To examine further the mechanism underlying aortic valve enlargement, we performed a fate-mapping of endothelial- (*Tie2-Cre;RosatdTomato*) and neural crest- (*Wnt1-Cre;RosatdTomato*)

Fig. 3. Abnormal aortic valve development occurs in targeted deletion of *Krox20* in the neural crest lineage. (A,B) Cross-sectional Hematoxylin and Eosin-stained aortic valves showing morphology in wild-type (WT, A) and *Wnt1-Cre;Krox20flox/flox* (B) mice. One example of bicuspid aortic valve observed in *Wnt1-Cre; Krox20flox/flox* (B) mutant mice, showing thickened and unequal-sized leaflets. Asterisks indicate valvular leaflets of the aortic valve. Arrowhead indicates a raphe between the right and non-coronary leaflets. (C,D) Three-dimensional (3D) reconstruction of histological images of E18.5 wild-type (C) and *Wnt1-Cre; Krox20flox/flox* (D) aortic valves, showing unequal-sized leaflets in *Wnt1-Cre;Krox20flox/flox* (D) mice. Note the raphe between the right and non-coronary leaflets (yellow). Left coronary (LC; blue), right coronary (RC; green), non-coronary (NC; purple), fused right coronary-non coronary (RC-NC) and raphe (yellow) leaflets. (E,F) Pulse-wave Doppler analysis from the aorta in 1-month-old wild-type (E) and *Wnt1-Cre;Krox20flox/flox* (F) mice. No significant aortic regurgitation is observed in wild-type mice (E; *n*=3), whereas a severe aortic insufficiency is found in *Wnt1-Cre;Krox20flox/flox* (F; *n*=3) mice. (G,H) Quantification of the thickness and the relative volume confirm an enlargement of the aortic valve in *Wnt1-Cre;Krox20flox/flox* and *Krox20lacZ/lacZ* compared with wild-type littermates. (I) Total nuclei per aortic valve leaflet were counted in wild-type and mutant embryos at E18.5, spanning a 180 μm depth. The mean of the total nuclei per leaflet demonstrates a significant increase in the *Wnt1-Cre; Krox20flox/flox* and *Krox20lacZ/lacZ* mice compared with wild-type littermates. All data were calculated from *n*=6 embryos for each genotype. Data mean±s.e.m. (*P<0.05, Student's *t*-test). BPM, beats per minute; RR, respiratory rate. Scale bars: 100 μm.

4

derivatives in wild-type and *Krox20*-null mutant embryos. At E18.5, *Tie2-Cre*-expressing endothelial cells were found at the same number in the aortic valve leaflets of *Krox20*^{−/−} and wild-type embryos (Fig. 4A-C). However, the number of neural crest-derived cells (*Wnt1-Cre*) was significantly increased (>1.8 fold; *P*<0.05) in the aortic valve leaflets of *Krox20*^{−/−} compared with wild-type littermates (Fig. 4D-F). At E18.5, quantification of Tomato-positive cells in the distinct leaflets shown additional neural crest-derived cells in the right and left coronary leaflets as well as in the non-coronary leaflet of *Krox20*^{−/−} aortic valve (Fig. S5). These data indicate that the abnormal aortic valve in *Krox20*^{−/−} embryos is associated with an increased number of neural crest-derived cells located in the valve leaflets.

We further examined the contribution of *Krox20*-derived cells using *Krox20*[Cre];*Rosa*[tdTomato] reporter mice. As *Krox20*[Cre] is a null allele, we analyzed the contribution of Krox20-Cre labeled cells in a heterozygous background (Voiculescu et al., 2000). To avoid the presence of two copies of the *Cre* gene in the homozygotes, leading to a higher initial expression relative to heterozygotes, we used *Krox20*[Cre/lacZ] compound mutant embryos. At E18.5, *Krox20*-null mutant embryos displayed higher number of *Krox20*-derived cells (Fig. 4G-I). Interestingly, the augmentation of *Wnt1-Cre*- and *Krox20-Cre*-labeled cell number was similar in the *Krox20*^{−/−} mutant embryos (compare Fig. 4F with 4I). Further analysis revealed singular accumulation of *Krox20*-derivatives in the non-coronary leaflet, although the coronary leaflets shown also moderate increase (Fig. S5). To assess whether this augmentation was associated with

higher proliferation, we counted phospho-histone H3 (PHH3) and Tomato double-positive cells in the three reported mice (Fig. 4J-L). Our results showed no defect in proliferation of valvular cells, confirming that higher numbers of neural crest-derived cells in *Krox20*^{−/−} valve leaflets is not due to excessive proliferation in the valve tissue. Together, these results suggest that accumulation of *Krox20-Cre*-labeled cells is caused by an earlier defective event.

As *Krox20* expression was detected in few endothelial-derived cells of the forming aortic valve (Fig. S3), we examined whether endothelial-specific deletion of *Krox20* can cause abnormal aortic valve development (Table 1; Fig. S6). At E18.5, anatomic and morphometric analyses of *Tie2-Cre;Krox20*[flox/flox] embryos shown no difference in the volume and thickness of the aortic valve leaflets when compared with control valves (Fig. S6). Surprisingly, a bicuspid was observed in 10% of the *Tie2-Cre;Krox20*[flox/flox] embryos (2/20) (Table 1). 3D reconstructions displayed two equal-sized leaflets without associated raphe (Fig. S6). These data suggest that BAV can also be observed when endothelial-specific deletion of *Krox20* occurs; however, the type of bifoliate valves was different from those observed in *Wnt1-Cre;Krox20*[flox/flox] embryos, without enlargement or excess cell numbers in the leaflets (Fig. S6).

Krox20-expressing neural crest cells contribute to the aortic valve leaflets

Krox20 controls and coordinates the formation of r3 and r5 territories (Schneider-Maunoury et al., 1993; Voiculescu et al., 2001).
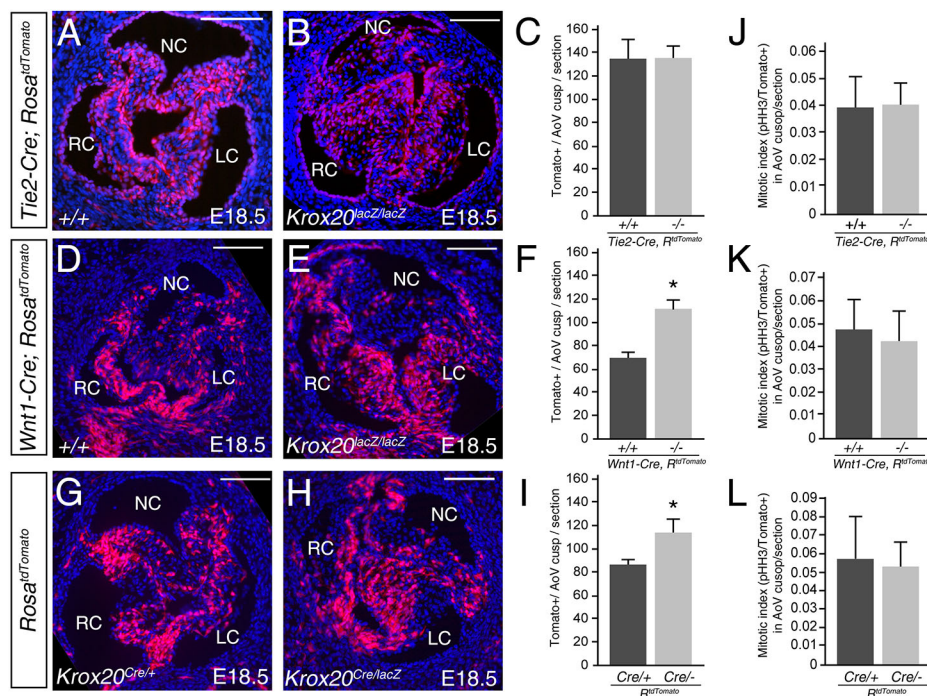

Fig. 4. Abnormal contribution of neural crest-derived cells in *Krox20*-null mice. (A,B,D,E,G,H) Fate-mapping of the endothelial, neural crest and *Krox20* lineages in the aortic valves of wild-type (WT, A,D), heterozygous (G) and *Krox20*-null (B,E,H) embryos at E18.5. (A-C) Immunofluorescence staining using *Tie2-Cre;Rosa*[tdTomato/+] reporter mice demonstrates normal contribution of endothelial cells in wild-type (A) and *Krox20*^{−/−} (B) littermate embryos. (C) Quantification confirms equivalent number of endothelial cells in wild-type (*n*=5) and mutant (*n*=5) embryos. (D-F) Immunofluorescence staining using *Wnt1-Cre;Rosa*[tdTomato/+] reporter mice shows an increased in the number of neural crest derivatives in the absence of *Krox20*. (F) Quantification of neural crest-derived cells demonstrates significant increase in *Krox20*^{−/−} (*n*=5) compared with wild-type (*n*=5) littermate embryos. (G-I) Immunofluorescence staining using *Krox20*[Cre];*Rosa*[tdTomato/+] reporter shows an increased in the number of *Krox20-Cre*-labeled cells in aortic valve leaflets of compound *Krox20*[Cre/lacZ] mutants compared with heterozygote *Krox20*[Cre/+] embryos. (I) Quantification of *Krox20-Cre*-labeled cells confirms the significant increase in *Krox20*-derived cells in *Krox20*[Cre/lacZ] (*n*=4) compared with *Krox20*[Cre/+] (*n*=4) littermate embryos. (J-L) Proliferation of Tomato-positive cells in the aortic valves evaluated using anti-phospho-Histone H3 (p-HH3). The mitotic index is the percentage of total p-HH3/Tomato-positive cells in 10 separate sections for three individuals of each genotype. The mitotic index shows no significant difference in *Tie2-Cre;Rosa*[tdTomato/+], *Wnt1-Cre;Rosa*[tdTomato/+] and *Krox20-Cre;Rosa*[tdTomato/+] reporter mice in wild-type and mutant embryos. Data are mean±s.e.m. (**P*<0.05, Student's *t*-test). LC, left coronary leaflet; NC, non-coronary leaflet; RC, right coronary leaflet. Scale bars: 100 μm.

Interestingly, *Krox20* expression is detected in NCCs migrating from r5 towards the 3rd pharyngeal arch (Fig. S2). However, this expression is transient as detection of the *Krox20* transcripts is low by E9.5 (Fig. S2). Comparison of *Krox20*-expressing cells with the *Wnt1*-positive population showed that both populations coincide (Fig. S7). To follow the fate of the r5-derived NCCs in the absence of a functional Krox20 protein, we used the compound mutant embryos *Krox20^{Cre/flox}*, which carry only one copy of the *Cre* gene (Taillebourg et al., 2002; Voiculescu et al., 2000). At E9.5, *lacZ* reporter gene activity in *Krox20^{Cre/+};R26R* embryos was detected in r3 and r5, and the derivatives of r5 neural crest that migrate toward the 3rd pharyngeal arch (Fig. 5A,B). Consistently, at E10.5, Tomato-positive cells were observed in the cardiac outflow tract of *Krox20^{Cre};Rosa^{tdTomato}* embryos (Fig. 5C). Subsequently, *Krox20-Cre*-labeled cells were detected in all leaflets of *Krox20^{Cre};Rosa^{tdTomato}* aortic valve (Fig. 5D-F). In *Krox20^{Cre/flox};R26R* embryos, a higher number of migrating NCCs were detected in the pharyngeal region at E9.5 (Fig. 5G,H). At E10.5, we found more *Krox20-Cre*-labeled cells in the outflow tract of homozygous than heterozygous embryos (Fig. 5I), consistent with additional *Krox20-Cre*-labeled cells detected in the aortic valve leaflets at later stages (Fig. 5J-L). At E13.5, quantification revealed an increased Tomato-positive cell number in aortic valve leaflets of *Krox20^{Cre/lacZ};*

Rosa^{tdTomato} embryos compared with *Krox20^{Cre/+};Rosa^{tdTomato}* heterozygous littermates, which was particularly obvious for the non-coronary leaflet (Fig. S8). Interestingly, in a homozygous background, *Krox20-Cre* labeled cells appeared misplaced within the leaflets (compared Fig. 5K,E), and due to the hyperplasia of the non-coronary leaflet, its sinus looked smaller in the mutant compared with controls (Fig. 5L, arrowhead). To further examine whether loss of Krox20 function in its own lineage can lead to aortic valve defect, we analyzed *Krox20^{Cre/flox}* mutant embryos. Analysis of *Krox20^{Cre/flox}* hypomorphic mutants revealed morphological anomalies of the aortic valve, including hyperplasic (13/13) and bicuspid (1/13) leaflets (Table 1), suggesting that reduction of *Krox20* expression in *Krox20*-expressing cells results to similar valve phenotype observed as for *Wnt1-Cre;Krox20^{flox/flox}* mutants.

To investigate the importance of the *Krox20-Cre*-labeled subpopulation of NCCs to aortic valve morphogenesis, we performed their genetic ablation in the mouse. For this purpose, we used the *Krox20^{GFP(DT)}* allele, in which the A chain of the diphtheria toxin (DT) is placed downstream of the floxed GFP sequence (Vermeren et al., 2003), where the DT is activated only upon Cre-mediated recombination (Fig. 5). *Krox20^{GFP(DT)/+}* mice were crossed with a *Wnt1-Cre* mice to obtain a specific depletion of *Krox20* derivatives and to avoid the early lethality linked to the
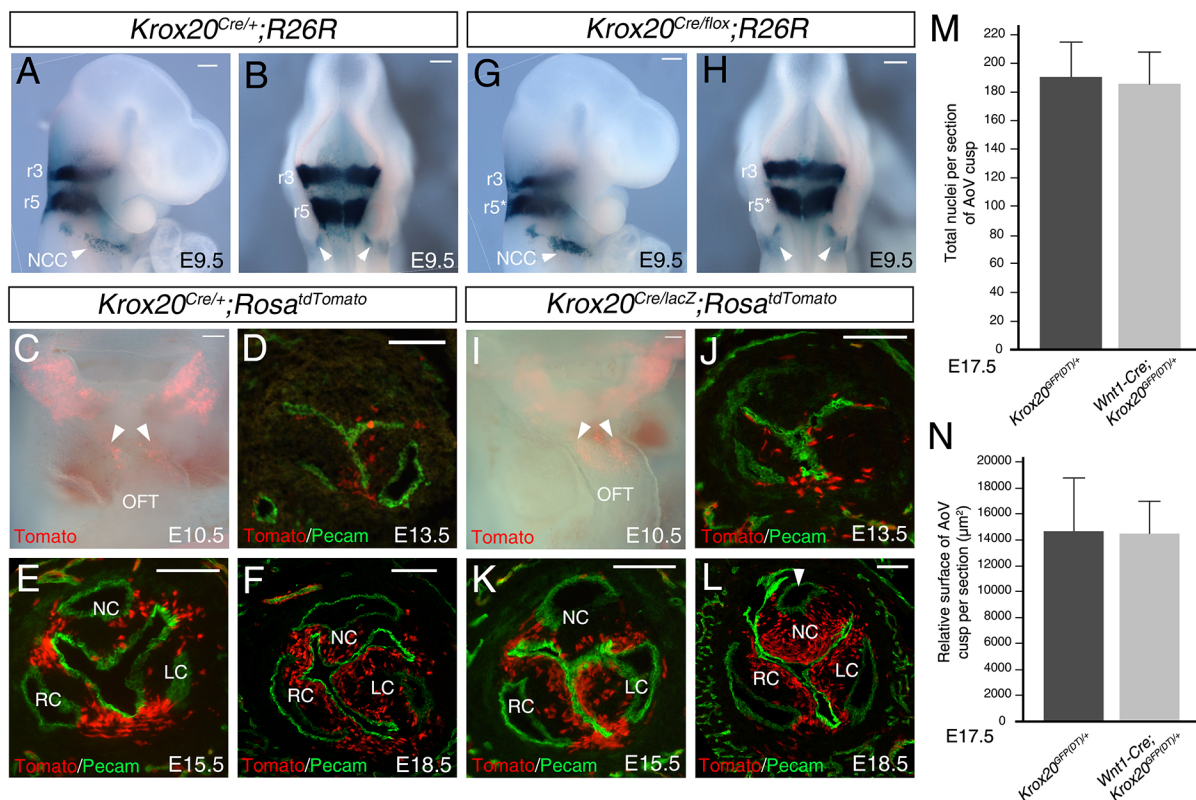
Fig. 5. Rhombomere 5 derivatives are affected in *Krox20* mutant mice. (A,B,G,H) X-gal staining on whole-mount embryos at E9.5 (A and G, right views; B and H, dorsal views), showing expression of the *Rosa26^{lacZ}* (*R26R*) reporter gene in heterozygous (A,B; *Krox20^{Cre/+}*) and compound homozygous mutant (G,H; *Krox20^{Cre/flox}*) mice. Transcriptional expression of *Krox20* is detected in rhombomere (r) 3 and r5, and in neural crest cells (NCCs, arrowheads). (C-F,I-L) Detection of the Tomato reporter protein in *Krox20^{Cre/+};Rosa^{tdTomato}* and *Krox20^{Cre/lacZ};Rosa^{tdTomato}* embryos. At E10.5, Tomato-positive cells (arrowheads in C,I) are observed into the cardiac outflow tract of both heterozygous (C) and homozygous mutant (I) embryos. Note the increased number of Tomato-positive cells in the outflow tract of *Krox20*-null embryos (I). (D-F,J-L) At E13.5, E15.5 and E18.5, Tomato-positive cells are significantly increased in *Krox20*-null (J-L) compared with heterozygous (D-F) embryos. Note the enlargement of the aortic valve leaflets in the *Krox20*-null embryos. Pecam is labeled in green. Arrowhead in L indicates valvar sinus. (M,N) Targeted expression of diphtheria toxin using *Wnt1-Cre;Krox20^{GFP(DT)/+}* embryos. (M) At E17.5, the total number of nuclei per section of aortic valve leaflets reveals no major difference between *Wnt1-Cre;Krox20^{GFP(DT)/+}* (*n*=4) and *Krox20^{GFP(DT)/+}* (*n*=5) embryos. (N) The relative surface area of the leaflets is indistinguishable between the *Krox20^{GFP(DT)/+}* and *Wnt1-Cre;Krox20^{GFP(DT)}* embryos. LC, left coronary leaflet; NC, non-coronary leaflet; OFT, outflow tract; RC, right coronary leaflet; RV, right ventricle. Scale bars: 200 μm in A,B,G,H; 100 μm in C-F,I-L.
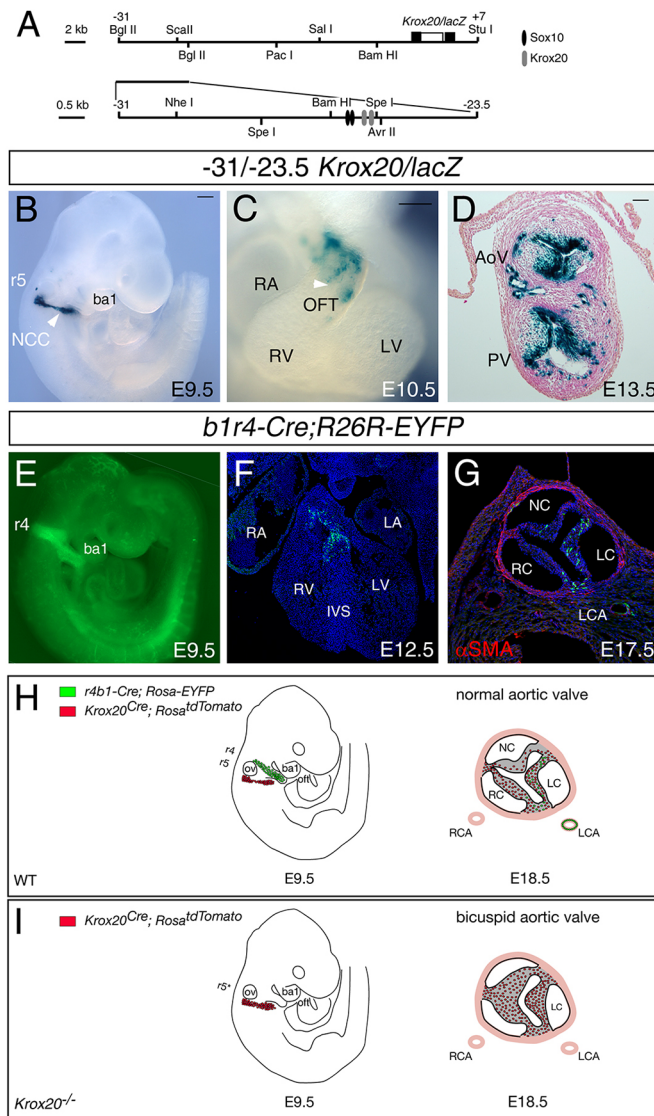
Fig. 6. Analysis of the NCE element of *Krox20* during arterial valve development. (A) Schematic representation showing the genomic region of *Krox20* and the −31/−23.5 *Krox20/lacZ* transgenic construct containing a *lacZ* in-frame insertion in *Krox20*. Restriction enzyme sites used to clone the genomic fragment are shown. Distances are in kb and indicate the position relative to the start site of transcription of *Krox20*. The conserved sequences and putative binding sites for Sox10 (black circles) and Krox20 (gray circles) are indicated. (B-D) *In vivo* analysis of the transgenic line −31/−23.5 *Krox20/lacZ* at E9.5 (B), E10.5 (C) and E13.5 (D). (B) At E9.5, β-galactosidase (β-gal) activity is detected in migratory neural crest cells (NCCs). (C) At E10.5, β-gal-positive cells (arrowhead) are observed in the outflow tract. (D) Transverse section through the outflow tract cushions at E13.5 shows β-gal-positive cells in the arterial valve leaflets. (E-G) Rhombomere (r) 4 fate mapping was performed on *b1r4-Cre; Rosa-EYFP* transgenic embryos (*n*=3). (E) At E9.5, b1r4-Cre-labeled cells are specifically detected in the r4 and the 2nd pharyngeal arch (ba). (F) At E12.5, section staining shows b1r4-Cre-labeled cells at the top of the interventricular septum (IVS). (G) At E17.5, a small number of b1r4-Cre-labeled cells are detected in the aortic valve. Note the presence of YFP-positive cells in the left coronary artery. αSMA (red) marks the smooth muscle cells. Nuclei are labeled with DAPI in blue. (H,I) Model depicting the contribution of a NCC population in normal aortic valve development (H) and its disruption in *Krox20−/−* embryos (I). (H) Distribution of NCCs migrating from rhombomere (r) 4 (*b1r4-Cre;Rosa-EYFP*; green) and r5 (*Krox20Cre;RosatdTomato*; red) in wild-type (WT) embryos. (I) In loss of *Krox20* function mutants, an excess of *Krox20*-derived neural crest cells leads to the swelling of the aortic valve leaflets. As a consequence, commissural fusion of the aortic valve leaflet occurs. AoV; aortic valve; ba1, 1st pharyngeal arch; IVS, interventricular septum; LA, left atrium; LCA, left coronary artery; LC, left coronary leaflet; LV, left ventricle; NC, non-coronary leaflet; OFT, outflow tract; ov, otic vesicle; PV, pulmonary valve; RA; right atrium; RC, right coronary leaflet; RCA, right coronary artery; RV, right ventricle. Scale bars: 200 μm in B,C; 50 μm in D.

One of the constructs studied, carrying sequences between −31 kb and −23.5 kb relative to the transcription start site of *Krox20* (−31/−23.5 *Krox20/lacZ*) was active in the neural crest (Fig. 6A). We used the −31/−23.5 *Krox20/lacZ* transgene to examine β-galactosidase pattern at different stages. At E9.5, X-gal staining showed that β-galactosidase-positive cells migrated from the r5 towards the 3rd pharyngeal arch region (Fig. 6B). By E10.5, reflecting the stability of the β-galactosidase protein, X-gal-stained cells were detected in the outflow tract and the arterial valve leaflets (Fig. 6C,D). These data identified the population of *Krox20*-expressing cells that are involved in arterial valve formation.

As our data indicate that r5 provides a population of migratory NCCs that contributes to the arterial valve leaflets, we asked whether a more cranial rhombomere such as r4 was also responsible for neural crest contribution to the arterial valves. We used the previously reported *b1r4-Cre;R26R-EYFP* transgenic mouse embryos to analysis r4-derived NCC contribution (Di Bonito et al., 2013). At E9.5, YFP-positive cells were detected in the r4 and the NCCs migrating towards the 2nd pharyngeal arch (Fig. 6E). At E12.5, EYFP-positive cells were detected at the top of the interventricular septum of the heart (Fig. 6F). At E17.5, we found very few YFP-positive cells in the left-coronary leaflet of the aortic valve (Fig. 6G). These results suggest that the contribution of pre-otic NCCs to the cardiac valves is distinct from that of post-otic NCCs, and that r5 constitutes the main source of NCC population that contribute to the arterial valves (Fig. 6H,I).

In conclusion, our data indicate that, in absence of functional Krox20 protein, additional neural crest-derived cells from r5 participates to the enlargement of the aortic valve leaflets (Fig. 6I), which may contribute to the fusion between two leaflets (R-N or L-N).

DISCUSSION
Our results identify neural crest-derived cells that contribute to arterial valve formation. The cardiac neural crest is a subpopulation of neural

elimination of all *Krox20*-expressing cells (Vermeren et al., 2003). In this condition, the elimination of these cells occurred around E9.5. At E17.5, the mesenchymal cells and relative surface were counted on several sections through the aortic valves of *Krox20GFP(DT)/+* and *Wnt1-Cre;Krox20GFP(DT)/+* embryos. Surprisingly, the analysis revealed no severe difference between *Wnt1-Cre;Krox20GFP(DT)/+* and *Krox20GFP(DT)/+* embryos (Fig. 5M,N), suggesting that killing the *Krox20*-expressing NCC population by the toxin was not sufficient to induce abnormality of the aortic valve, which can be explained by replacement of depleted NCCs by passive migration of surrounding cells into the 'gap' – a region devoid of cells – as already reported in other neural crest ablation studies (Vaglia and Hall, 1999). Consistently, *in situ* hybridization experiments with *Crabp1*, a marker of NCCs, showed an abnormal, but still present, post-otic stream of NCCs migrating toward the 3rd and 4th pharyngeal aortic arch of *Wnt1-Cre;Krox20GFP(DT)/+* embryos (Fig. S9).

The *Krox20* NCE element marks the NCC population that contributes to aortic valve leaflets
Previous studies have identified a cis-acting enhancer element (NCE) located upstream of the *Krox20* gene that can recapitulate its neural crest pattern in transgenic mice (Ghislain et al., 2003, 2002).

crest that located in the neural folds spanning from the middle of the otic placode to the caudal border of somite 3, corresponding to rhombomeres (r) 6, 7 and 8 (Kirby, 2007). Studies in chick and mouse embryos have shown that cardiac NCCs contribute to the arterial valves (de Lange et al., 2004; Jiang et al., 2000; Waldo et al., 1998). More recently, Arima and colleagues (2012) have identified the contribution of pre-otic cranial neural crest to developing coronary arteries and adjacent cardiac tissues (Arima et al., 2012). In this study, quail-chick chimera experiments made with neural crest between the midbrain and pre-otic hindbrain (r1-r5) showed the presence of quail-positive cells primarily in the interventricular septum but not in the arterial valves. Pre-otic neural crest ablation resulted in defects in coronary arteries, but not in valve defects, indicating that, at least in the chick embryo, neural crest cells derived from r1 to r5 are not crucial for arterial valve formation (Arima et al., 2012). Lack of direct evidence has led many investigators to question which neural crest region contributes to valve development. Our present findings provide direct evidence by identifying a specific subpopulation of NCCs derived from r5 as a source of arterial valve crest. In particular, NCCs expressing *Krox20* contribute to the insertion zone of the valve leaflets and the interleaflet triangle between each leaflet. Consistently, a recent study showed that the interleaflet triangle fibrous tissues derived from the outflow cushions region have contribution from NCCs (Richardson et al., 2017).

Previous studies have identified expression of *Krox20* in r3 and r5, and shown that its expression is important for patterning of the hindbrain (Ghislain et al., 2003; Schneider-Maunoury et al., 1993; Voiculescu et al., 2001). In the neural crest, *Krox20* expression is mainly restricted to cells migrating lateral to r5 towards the 3rd pharyngeal arch and presumably originating from r5 (Schneider-Maunoury et al., 1993). In addition, a *Krox20* neural crest-specific element (NCE) has been characterized that drives expression of the reporter *lacZ* gene in NCCs emigrating from r5 in transgenic mice (Ghislain et al., 2003, 2002). Our lineage-tracing analysis showed that $Krox20^{Cre}$ labeled cells are detected in outflow tract cushions and subsequently in the aortic valve, which reproduced the profile of the −31/−23.5 *Krox20/lacZ* (NCE) transgene, suggesting that NCCs emigrating from r5 contribute to arterial valve formation. Interestingly, a study in the chick suggested that *Krox20* expression in pharyngeal neural crest does not correlate with rhombomeric segmentation, and that there may be intrinsic differences in regulation between the r5 and r6 *Krox20*-expressing population (Nieto et al., 1995). The same study demonstrated that *Krox20* expression occurs in neural crest precursors not only in r5, but also in r6, and that both of these precursor populations contribute to the stream of *Krox20*-expressing NCCs (Nieto et al., 1995). Detailed analysis of the fate of prospective r5 cells in *Krox20* mutant mice using molecular markers demonstrated that a large part of r5 cells acquire even-numbered rhombomere characters in *Krox20*-null embryos (Voiculescu et al., 2001). Our lineage-tracing analysis in compound $Krox20^{Cre/flox}$ null embryos revealed an increase in the number of migrating NCCs, suggesting that acquisition of r6 identity disturbs the neural crest migration. Furthermore, the increased number of migrating NCCs is likely to contribute to the hyperplasia of the aortic valves observed in *Krox20* mutant. These findings lead us to speculate that neural crest arising from r5 provides important information for valve development.

The identification of the NCE transcriptional enhancer as a regulatory element expressed in r5-derived NCCs raises the question how is *Krox20* expression regulated in these cells? The −31/−23.5 *Krox20/lacZ* transgene reporter used in our study to mark the NCCs that contribute to the arterial valves comprises a 1 kb fragment

(−26.5 kb to −25.5 kb) that contains *Krox20*-binding sites necessary for its autoregulation in the NCCs (Ghislain et al., 2003). Interestingly, the same fragment contains two adjacent, head-to-head, HMG box-binding sites for two members of the HMG box group expressed in the pre- and post-migratory NCCs: Sox10 and Sox9. Ghislain et al. (2003) have reported that Sox10 is a crest-specific factor essential for *Krox20* autoregulation in NCCs (Ghislain et al., 2003). Although several studies have reported expression of *Sox10* in the valve and a contribution of *Sox10*-Cre labeled cells to the heart, no cardiac defects have yet been reported in Sox10 mutant embryos (Montero et al., 2002; Simon et al., 2012). Interestingly, a double outlet right ventricle, which occurs when outflow tract septation is malformed, has been reported in one patient carrying a deletion at the *SOX10* locus (Bondurand et al., 2007). Together, these data suggest that Sox10 is an important regulator of migrating NCCs, including the subpopulation of neural crest expressing *Krox20*.

In human patients, the most frequent BAV subtypes result from fusion of either the left coronary and right coronary leaflets (R-L) or the right coronary and non-coronary leaflets (R-N) (Sievers and Schmidtke, 2007). A recent study using mouse and Syrian hamster as animal models suggested that R-N and R-L BAVs could have distinct embryological origins; R-N BAVs would result from defective development of the outflow tract cushions, whereas R-L BAVs would result from abnormal septation of proximal outflow tract region associated with defective NCC behavior (Fernández et al., 2009). However, the precise role of NCCs in the formation of the arterial valves remained unclear until a recent study showed that the aggregation of NCCs, once they enter the outflow tract cushions, is important to define how the arterial leaflets form after outflow tract septation (Phillips et al., 2013). Thus, the position of NCCs is crucial for the pattern of aortic valve leaflets. Deletion of *Krox20* results in R-N or L-N subtypes, suggesting abnormal development of outflow tract cushions. However, we never observed abnormal great arteries in $Krox20^{−/−}$ embryos, and the BAV phenotype is only detected after E15.5. These findings suggest that fusion between two leaflets may occur late in valve development. Although the phenotype in the $Krox20^{−/−}$ null and $Krox20^{Cre/flox}$ hypomorphic embryos is likely to result from a combination of requirement for *Krox20* in neural crest- and endothelial-derived cells, we always observed an enlargement of the arterial valve similar to those observed in the $Wnt1-Cre;Krox20^{flox/flox}$ embryos. Our lineage-tracing analysis shows that this enlargement is caused by addition of *Krox20* derivatives. Additional *Krox20*-Cre-labeled cells appear misplaced in the leaflet, which may explain the phenotype of bifoliate valves. Our previous study demonstrated that Krox20 is a key regulator of fibrillar *Col1a1* and *Col3a1* genes (Odelin et al., 2014). In addition, we have detected a reduction of collagen fibers and an increase of proteoglycan proteins in $Krox20^{−/−}$ aortic valves. Thus, the hyperplasia observed in *Krox20* mutants is associated with a myxomatous-like phenotype. Therefore, modification of the extracellular matrix at the insertion zone of the arterial valve leaflets would lead to a widening and loss of delimitation of these insertion zones at the time of the excavation phase. The insertion zone would no longer be dense enough to maintain the endothelium close to the aortic wall, leading to the fusion of two layers during valvular maturation. Thus, an odd maturation of the valve could lead to the abnormal development of the aortic valve, such as BAV. Interestingly, commissural fusion of the native aortic valve leaflets occurs frequently in individuals supported by a continuous axial flow left ventricular assist device (Gallen et al., 2012; Mudd et al., 2008), suggesting that fusion between two

leaflets can happen during adulthood depending on environmental events affecting flow in the arterial valves.

Gene expression and lineage-tracing analyses revealed endogenous expression of *Krox20* in the forming aortic valve (Odelin et al., 2014). Here, we confirm that very few neural crest- and endothelial-derived cells express Krox20 in the aortic valve at E18.5 (Fig. S3). Interestingly, mice with neural crest-specific deletion of *Krox20* have less BAV (10.5%) than *Krox20*$^{-/-}$ mice (27%), suggesting additional contributions (Table 1). Endothelial-specific deletion of *Krox20* leads to BAV phenotype (10%) (Table 1). However, our morphometric analysis demonstrates that aortic valve leaflets are not hyperplastic in this context and BAV are formed by equally sized leaflets (Fig. S6). Collectively, these findings indicate contribution of *Krox20*-expressing endothelial cells during arterial valve development; however, additional studies are needed to further clarify the function of Krox20 in the endothelial cells. In conclusion, our data highlight the role of NCCs in aortic valve disease and provide a new model to understand the pathophysiology of the bicuspid phenotype.

MATERIALS AND METHODS

Mice

All animal procedures were carried out under protocols approved by a national appointed ethical committee for animal experimentation (Ministère de l'Education Nationale, de l'Enseignement Supérieur et de la Recherche; Authorization N° 2931-2015113016228473). The *Krox20*^{lacZ}, *Krox20*$^{GFP(DT)}$, *Krox20*^{flox} and *Krox20*^{Cre} alleles have been previously described (Schneider-Maunoury et al., 1993; Taillebourg et al., 2002; Vermeren et al., 2003; Voiculescu et al., 2000). The *Gt(ROSA)26Sor*^{tm1Sor} (*R26R*), *Gt(ROSA)26Sor*$^{tm4(ACTB-tdTomato,-EGFP)Luo}$ (*Rosa*$^{Tomato-GFP}$), *Gt(ROSA)26Sor*$^{tm9(CAG-tdTomato)Hze}$ (*Rosa*^{tdTomato}), *Gt(ROSA)26Sor*$^{tm1(EYFP)Cos}$ (*R26R-EYFP*) and *Z/AP* transgenic lines have been previously described (Lobe et al., 1999; Madisen et al., 2010; Muzumdar et al., 2007; Soriano, 1999; Srinivas et al., 2001). The *Tg(Tek-cre)1Ywa* (*Tie2-Cre*), *Wnt1-Cre* and *b1r4-Cre* mice have been previously described (Di Bonito et al., 2013; Jiang et al., 2000; Kisanuki et al., 2001). *Krox20*$^{flox/+}$ or *Krox20*$^{lacZ/+}$ mice were maintained on a C57Bl/6 background and inter-crossed with *Tie2-Cre*, *Wnt1-Cre* or *Krox20*^{Cre} to generate heterozygous offspring that were obtained at expected Mendelian ratios. The −31 kb to −23.5 kb *Krox20/lacZ* transgene has been previously described by Ghislain et al. (2003). Transgenic mice were generated after revitalization of frozen eggs. After echocardiography analysis, adult *Wnt1-Cre;Krox20*$^{flox/flox}$ mice were sacrificed via intra-peritoneal injection of sodium pentobarbital (0.5 ml). Timed litters were collected at embryonic day (E) 9.5 to E18.5, counting evidence of a vaginal plug as E0.5.

Histological and immunostaining

Standard histological procedures were used (Ryckebusch et al., 2010). Heart tissues from *Krox20*$^{-/-}$ or *Krox20c*^{KO} and littermate controls were fixed in neutral-buffered 4% paraformaldehyde in PBS, rinsed, dehydrated, paraffin-embedded and tissue sections cut at 8 µm. Sections were stained with Harris' Hematoxylin and Eosin (Sigma). AP2α (1:500, clone 3B5 DHSB), αSMA (1:500, Sigma, F3777), CD31 (1:100, Pharmingen, 01951A), GFP (1:500, Invitrogen, A11122), Krox20 (1:100, Covance, PRP-236P), and phospho-histone H3 (1:100, Millipore, 06-570) immunofluorescence were performed using Alexa fluorescent dye-conjugated secondary antibodies (Life Technologies) at 1:500. Nuclei were labeled with DAPI.

In situ hybridization and X-gal staining

X-gal staining and *in situ* hybridization were performed on whole-mount embryos or 12 µm frozen sections as described previously (Odelin et al., 2014). For each experiment, a minimum of three embryos of each genotype was observed. Embryos were examined using an AxioZoom.V16 (Zeiss) and photographed with an Axiocam digital camera (Zen 2011, Zeiss).

Quantification of valve anomalies

Quantification of valve thickness: the leaflets of the valves were used over a minimum depth of 100 µm using a DM5000 Leica microscope with LAS software. ImageJ software was used to measure the surface of the valve and the number of nuclei labeled by DAPI. Measurements were performed on at least ten different sections per leaflet. The values were averaged. A minimum number of six animals were used per genotype.

Three-dimensional (3D) reconstructions: Fiji software was used to make the 3D reconstructions presented. At E18.5, images of 20-30 8 µm paraffin sections were manually aligned to generate 3D reconstruction. Volumetric measurements of the aortic valve are presented as the average of six reconstructions of each genotype.

Echocardiography

In vivo valve structure and function of *Wnt1-Cre;Krox20*$^{flox/flox}$ mice were evaluated using a high-frequency scanner (Vevo2100 VisualSonics) as previously described (Odelin et al., 2014). Briefly, 1-month-old mice were anesthetized with 1-2% isofluorane inhalation and placed on a heated platform to maintain temperature during the analysis. Two-dimensional imaging was recorded with a 22-55 MHz transducer (MS550D) to capture long- and short-axis projections with guided M-Mode, B-Mode and color and pulsed-wave Doppler. Doppler interrogation was performed on the arterial valve outflow in the parasternal long-axis view to assess aortic flow, using a sample volume toggle to optimize the angle of interrogation. Aortic insufficiency was defined as valve incompetence with reversal of flow in diastole.

References

Arima, Y., Miyagawa-Tomita, S., Maeda, K., Asai, R., Seya, D., Minoux, M., Rijli, F. M., Nishiyama, K., Kim, K.-S., Uchijima, Y. et al. (2012). Preotic neural crest cells contribute to coronary artery smooth muscle involving endothelin signalling. *Nat. Commun.* **3**, 1267.

Bondurand, N., Dastot-Le Moal, F., Stanchina, L., Collot, N., Baral, V., Marlin, S., Attie-Bitach, T., Giurgea, I., Skopinski, L., Reardon, W. et al. (2007). Deletions at the SOX10 gene locus cause Waardenburg syndrome types 2 and 4. *Am. J. Hum. Genet.* **81**, 1169-1185.

de Lange, F. J., Moorman, A. F., Anderson, R. H., Manner, J., Soufan, A. T., de Gier-de Vries, C., Schneider, M. D., Webb, S., van den Hoff, M. J. and Christoffels, V. M. (2004). Lineage and morphogenetic analysis of the cardiac valves. *Circ. Res.* **95**, 645-654.

Di Bonito, M., Narita, Y., Avallone, B., Sequino, L., Mancuso, M., Andolfi, G., Franzè, A. M., Puelles, L., Rijli, F. M. and Studer, M. (2013). Assembly of the auditory circuitry by a Hox genetic network in the mouse brainstem. *PLoS Genet.* **9**, e1003249.

Eisenberg, L. M. and Markwald, R. R. (1995). Molecular regulation of atrioventricular valvuloseptal morphogenesis. *Circ. Res.* **77**, 1-6.

Fedak, P. W. M., Verma, S., David, T. E., Leask, R. L., Weisel, R. D. and Butany, J. (2002). Clinical and pathophysiological implications of a bicuspid aortic valve. *Circulation* **106**, 900-904.

Fernández, B., Durán, A. C., Fernández-Gallego, T., Fernández, M. C., Such, M., Arqué, J. M. and Sans-Coma, V. (2009). Bicuspid aortic valves with different spatial orientations of the leaflets are distinct etiological entities. *J. Am. Coll. Cardiol.* **54**, 2312-2318.

Gallen, T. B., Lau, W. T. and Mehta, A. R. (2012). Complete aortic valve fusion after HeartMate II left ventricular assist device support. *J. Cardiothorac. Vasc. Anesth.* **26**, 1060-1062.

Garg, V. (2006). Molecular genetics of aortic valve disease. *Curr. Opin. Cardiol.* **21**, 180-184.

Ghislain, J., Desmarquet-Trin-Dinh, C., Jaegle, M., Meijer, D., Charnay, P. and Frain, M. (2002). Characterisation of cis-acting sequences reveals a biphasic, axon-dependent regulation of Krox20 during Schwann cell development. *Development* **129**, 155-166.

Ghislain, J., Desmarquet-Trin-Dinh, C., Gilardi-Hebenstreit, P., Charnay, P. and Frain, M. (2003). Neural crest patterning: autoregulatory and crest-specific elements co-operate for Krox20 transcriptional control. *Development* **130**, 941-953.

Hinton, R. B. and Yutzey, K. E. (2011). Heart valve structure and function in development and disease. *Annu. Rev. Physiol.* **73**, 29-46.

Hoffman, J. I. E. and Kaplan, S. (2002). The incidence of congenital heart disease. *J. Am. Coll. Cardiol.* **39**, 1890-1900.

Jain, R., Engleka, K. A., Rentschler, S. L., Manderfield, L. J., Li, L., Yuan, L. and Epstein, J. A. (2011). Cardiac neural crest orchestrates remodeling and functional maturation of mouse semilunar valves. *J. Clin. Invest.* **121**, 422-430.

Jiang, X., Rowitch, D. H., Soriano, P., McMahon, A. P. and Sucov, H. M. (2000). Fate of the mammalian cardiac neural crest. *Development* **127**, 1607-1616.

Kirby, M. L. (2007). *Cardiac Development*. Oxford, University Press.

Kirby, M. L., Gale, T. F. and Stewart, D. E. (1983). Neural crest cells contribute to normal aorticopulmonary septation. *Science* **220**, 1059-1061.

Kisanuki, Y. Y., Hammer, R. E., Miyazaki, J.-I., Williams, S. C., Richardson, J. A. and Yanagisawa, M. (2001). Tie2-Cre transgenic mice: a new model for endothelial cell-lineage analysis in vivo. *Dev. Biol.* **230**, 230-242.

Kuratani, S. C. and Kirby, M. L. (1991). Initial migration and distribution of the cardiac neural crest in the avian embryo: an introduction to the concept of the circumpharyngeal crest. *Am. J. Anat.* **191**, 215-227.

Le Douarin, N. M. and Teillet, M. A. (1973). The migration of neural crest cells to the wall of the digestive tract in avian embryo. *J. Embryol. Exp. Morphol.* **30**, 31-48.

Le Lievre, C. S. and Le Douarin, N. M. (1975). Mesenchymal derivatives of the neural crest: analysis of chimaeric quail and chick embryos. *J. Embryol. Exp. Morphol.* **34**, 125-154.

Lewis, A. E., Vasudevan, H. N., O'Neill, A. K., Soriano, P. and Bush, J. O. (2013). The widely used Wnt1-Cre transgene causes developmental phenotypes by ectopic activation of Wnt signaling. *Dev. Biol.* **379**, 229-234.

Lincoln, J., Alfieri, C. M. and Yutzey, K. E. (2004). Development of heart valve leaflets and supporting apparatus in chicken and mouse embryos. *Dev. Dyn.* **230**, 239-250.

Lobe, C. G., Koop, K. E., Kreppner, W., Lomeli, H., Gertsenstein, M. and Nagy, A. (1999). Z/AP, a double reporter for cre-mediated recombination. *Dev. Biol.* **208**, 281-292.

Madisen, L., Zwingman, T. A., Sunkin, S. M., Oh, S. W., Zariwala, H. A., Gu, H., Ng, L. L., Palmiter, R. D., Hawrylycz, M. J., Jones, A. R. et al. (2010). A robust and high-throughput Cre reporting and characterization system for the whole mouse brain. *Nat. Neurosci.* **13**, 133-140.

Montero, J. A., Giron, B., Arrechedera, H., Cheng, Y.-C., Scotting, P., Chimal-Monroy, J., Garcia-Porrero, J. A. and Hurle, J. M. (2002). Expression of Sox8, Sox9 and Sox10 in the developing valves and autonomic nerves of the embryonic heart. *Mech. Dev.* **118**, 199-202.

Mudd, J. O., Cuda, J. D., Halushka, M., Soderlund, K. A., Conte, J. V. and Russell, S. D. (2008). Fusion of aortic valve commissures in patients supported by a continuous axial flow left ventricular assist device. *J. Heart Lung Transplant.* **27**, 1269-1274.

Muzumdar, M. D., Tasic, B., Miyamichi, K., Li, L. and Luo, L. (2007). A global double-fluorescent Cre reporter mouse. *Genesis* **45**, 593-605.

Nakamura, T., Colbert, M. C. and Robbins, J. (2006). Neural crest cells retain multipotential characteristics in the developing valves and label the cardiac conduction system. *Circ. Res.* **98**, 1547-1554.

Nieto, M. A., Sechrist, J., Wilkinson, D. G. and Bronner-Fraser, M. (1995). Relationship between spatially restricted Krox-20 gene expression in branchial neural crest and segmentation in the chick embryo hindbrain. *EMBO J.* **14**, 1697-1710.

Odelin, G., Faure, E., Kober, F., Maurel-Zaffran, C., Théron, A., Coulpier, F., Guillet, B., Bernard, M., Avierinos, J.-F., Charnay, P. et al. (2014). Loss of Krox20 results in aortic valve regurgitation and impaired transcriptional activation of fibrillar collagen genes. *Cardiovasc. Res.* **104**, 443-455.

Person, A. D., Klewer, S. E. and Runyan, R. B. (2005). Cell biology of cardiac cushion development. *Int. Rev. Cytol.* **243**, 287-335.

Phillips, H. M., Mahendran, P., Singh, E., Anderson, R. H., Chaudhry, B. and Henderson, D. J. (2013). Neural crest cells are required for correct positioning of the developing outflow cushions and pattern the arterial valve leaflets. *Cardiovasc. Res.* **99**, 452-460.

Richardson, R., Eley, L., Donald-Wilson, C., Davis, J., Curley, N., Alqahtani, A., Murphy, L., Anderson, R. H., Henderson, D. J. and Chaudhry, B. (2017). Development and maturation of the fibrous components of the arterial roots in the mouse heart. *J. Anat.* (in press).

Ryckebusch, L., Bertrand, N., Mesbah, K., Bajolle, F., Niederreither, K., Kelly, R. G. and Zaffran, S. (2010). Decreased levels of embryonic retinoic acid synthesis accelerate recovery from arterial growth delay in a mouse model of DiGeorge syndrome. *Circ. Res.* **106**, 686-694.

Sauka-Spengler, T. and Bronner, M. (2010). Snapshot: neural crest. *Cell* **143**, 486-486.

Schneider-Maunoury, S., Topilko, P., Seitanidou, T., Levi, G., Cohen-Tannoudji, M., Pournin, S., Babinet, C. and Charnay, P. (1993). Disruption of Krox-20 results in alteration of rhombomeres 3 and 5 in the developing hindbrain. *Cell* **75**, 1199-1214.

Sievers, H.-H. and Schmidtke, C. (2007). A classification system for the bicuspid aortic valve from 304 surgical specimens. *J. Thorac. Cardiovasc. Surg.* **133**, 1226-1233.

Simon, C., Lickert, H., Götz, M. and Dimou, L. (2012). Sox10-iCreERT2: a mouse line to inducibly trace the neural crest and oligodendrocyte lineage. *Genesis* **50**, 506-515.

Siu, S. C. and Silversides, C. K. (2010). Bicuspid aortic valve disease. *J. Am. Coll. Cardiol.* **55**, 2789-2800.

Soriano, P. (1999). Generalized lacZ expression with the ROSA26 Cre reporter strain. *Nat. Genet.* **21**, 70-71.

Srinivas, S., Watanabe, T., Lin, C.-S., William, C. M., Tanabe, Y., Jessell, T. M. and Costantini, F. (2001). Cre reporter strains produced by targeted insertion of EYFP and ECFP into the ROSA26 locus. *BMC Dev. Biol.* **1**, 4.

Taillebourg, E., Buart, S. and Charnay, P. (2002). Conditional, floxed allele of the Krox20 gene. *Genesis* **32**, 112-113.

Vaglia, J. L. and Hall, B. K. (1999). Regulation of neural crest cell populations: occurrence, distribution and underlying mechanisms. *Int. J. Dev. Biol.* **43**, 95-110.

Vermeren, M., Maro, G. S., Bron, R., McGonnell, I. M., Charnay, P., Topilko, P. and Cohen, J. (2003). Integrity of developing spinal motor columns is regulated by neural crest derivatives at motor exit points. *Neuron* **37**, 403-415.

Voiculescu, O., Charnay, P. and Schneider-Maunoury, S. (2000). Expression pattern of a Krox-20/Cre knock-in allele in the developing hindbrain, bones, and peripheral nervous system. *Genesis* **26**, 123-126.

Voiculescu, O., Taillebourg, E., Pujades, C., Kress, C., Buart, S., Charnay, P. and Schneider-Maunoury, S. (2001). Hindbrain patterning: Krox20 couples segmentation and specification of regional identity. *Development* **128**, 4967-4978.

Waldo, K., Miyagawa-Tomita, S., Kumiski, D. and Kirby, M. L. (1998). Cardiac neural crest cells provide new insight into septation of the cardiac outflow tract: aortic sac to ventricular septal closure. *Dev. Biol.* **196**, 129-144.

Wilkinson, D. G., Bhatt, S., Chavrier, P., Bravo, R. and Charnay, P. (1989). Segment-specific expression of a zinc-finger gene in the developing nervous system of the mouse. *Nature* **337**, 461-464.